https://doi.org/10.5194/egusphere-2026-2006
Preprint. Discussion started: 22 May 2026

Global radiative forcing of stratospheric aerosols injected by the 2020 Australian extreme wildfire event

Raphaël Lebrun[1,2], Yevgeny Derimian [1], François Ravetta [2], Jérôme Bureau [2], and Sergey Khaykin [2]

[1]Laboratoire d'Optique Atmosphérique, CNRS, Université de Lille, Villeneuve d'Ascq, France
[2]Laboratoire Atmosphères, Observations Spatiales, IPSL, CNRS, Sorbonne Université, Paris, France

Correspondence: Raphaël Lebrun (raphael.lebrun@ipsl.fr), Yevgeny Derimian (yevgeny.derimian@univ-lille.fr), and Sergey Khaykin (sergey.khaykin@latmos.ipsl.fr)

Abstract. During the last decades, extreme wildfires have injected large amounts of biomass-burning aerosols in the stratosphere. Partly composed of carbon, these aerosols absorb incoming solar radiation, inducing changes in the atmosphere's energy balance, and can self-loft to altitudes higher than 30 km, with an increased residence time of several months. In this study we estimate the radiative forcing of stratospheric aerosols from the Australian New Year Super Outbreak (ANYSO) in 2020. We first model individual self-lofting plumes from the Pacific Northwest Event (PNE) in Canada in 2017 and from ANYSO to constrain the aerosols' optical properties. We use observations to track them and model their heating rates. For the PNE plume a Single Scattering Albedo (SSA) of 0.95 is the best estimate to compute the heating rates, as well as a SSA of 0.90 - 0.95 for the ANYSO plume. Cloud cover and geometrical thickness of the plume have a crucial impact on these computations. We then compute the direct radiative forcing of Southern Hemisphere aerosols injected in the stratosphere by ANYSO in 2020. Cloud cover has a crucial impact on those forcings, especially at the top of the atmosphere (TOA) where it makes values ranging from negative (clear-sky) to positive (all-sky). The global TOA radiative forcing of stratospheric aerosols from ANYSO over 2020 was evaluated at 0.08 to 0.19 W.m^2 in all-sky, and -0.17 to -0.12 W.m^2 in clear-sky. The surface radiative forcing estimate is -0.04 to -0.06 W.m^2 in all-sky and -0.29 to -0.24 W.m^2 in clear-sky.

1 Introduction

During the last couple of decades, intense pyrocumulonimbus (PyroCb) activity was observed during extreme wildfire events (Fromm et al. (2010); Peterson et al. (2025)). In some of these cases, stratospheric injections of biomass burning aerosols by PyroCb were observed (Christian et al. (2019); Khaykin et al. (2020)), and the mass of aerosols injected in the stratosphere sometimes reached levels comparable to medium-size volcanic eruptions (Peterson et al. (2018)). Black carbon and organic carbon being part of the composition of the biomass-burning aerosols, they absorb incoming solar radiation and locally warm the atmosphere. The temperature changes induced by these injections in the stratosphere can cause local vorticity anomalies, leading to parts of the plume to become vorticized (Smoke Charged Vortices (SCVs), Allen et al. (2020); Khaykin et al. (2025)), increasing their residence time in the stratosphere, aerosol concentration and optical thickness (Kablick III et al. (2020); Lestrelin et al. (2021)). This absorption of the solar radiation can also uplift the SCVs in the atmosphere by diabatic heating. This process called self-lofting has been observed (Boers et al. (2010); de Laat et al. (2012)), with SCVs injected at

https://doi.org/10.5194/egusphere-2026-2006
Preprint. Discussion started: 22 May 2026

15km self-lofting up to 35km, with a time residency in the stratosphere of several months (Allen et al. (2020); Khaykin et al. (2020)).

The global radiative forcing of these stratospheric injections has been studied, but the wide variety of assumptions made in the different studies make these results difficult to compare. For the PNE (Pacific Northwest Event which corresponds to Canadian fires in the summer of 2017), Das et al. (2021) found, for the stratospheric aerosol injections, a global, all-sky, SW (shortwave) radiative forcing (RF) of -0.03 W.m^{-2} at TOA (Top Of the Atmosphere), Christian et al. (2019) found 0.02 W.m^{-2} and Lee et al. (2023) found 0.196 W.m^{-2}. For the ANYSO (Australian New Year Super Outbreak), Heinold et al. (2022) found a SW TOA RF of 0.37-0.5 W.m^{-2} in all-sky conditions, while Khaykin et al. (2020) and Sellitto et al. (2022) respectively found -0.31 and -0.35 W.m^{-2} in clear-sky conditions. The discrepancies between these different results are caused by the different assumptions made regarding the composition of the aerosols, the radiative models being used, or the presence of clouds.

In this study we aim at computing the global radiative forcings of the stratospheric injection by ANYSO over 2020. To do so we first want to better understand the composition of the aerosols and their radiative properties, as well as the impact of various background parameters involved in the radiative transfer, including cloud cover and surface albedo. The remote sensing methods used to observe these stratospheric aerosols are not yet able to precisely quantify their absorption properties and uncertainties remain. To tackle this issue, several studies have considered external mixing and tried to constrain the organic carbon to black carbon ratio of these aerosols, with consistent values in the range of OC/BC=2-3% (Yu et al., 2019; Torres et al., 2020; Das et al., 2021; Yu et al., 2021; Guimond et al., 2023; Lee et al., 2023). Before computing radiative forcings we will first use well-observed self-lofting SCVs to constrain the optical properties of the aerosols. Having access to the heating rates observed for these SCVs, can we reproduce them using radiative transfer modeling tools ? If so, which SSA allows us to better represent the observed heating rates ? Having studied these individual well-identified self-lofting plumes, we then apply our method to compute the global radiative forcings of the stratospheric aerosols injected by ANYSO in 2020.

In Section 2, we present the studied datasets as well as the radiative methodology used to model the self-lofting of the SCVs and the radiative forcings of stratospheric aerosols. We present our results in Section 3 where we first compute sensitivities of the heating rates to different parameters to understand the impact of microphysical properties of the aerosols on the self-lofting process, as well as that of the environment of the plumes. We then present heating rates values computed both in clear-sky and all-sky conditions, and discuss the range of SSA values derived for each case. We then use a global dataset of observations for stratospheric aerosols in 2020 to estimate the global radiative forcing of the injection by ANYSO, both in clear-sky and all-sky conditions. We also present the radiative forcings computed for an individual SCV. In Section 4 we summarize our results and present some perspectives going forward.

https://doi.org/10.5194/egusphere-2026-2006
Preprint. Discussion started: 22 May 2026

2 Datasets and method

2.1 Observations by CALIOP and OMPS-LP : tracking the plumes from PNE and ANYSO

In this section we focus on the particular cases of self-lofting SCVs to acquire a better understanding of important parameters at stake in the radiative process of self-lofting, and to better constrain the optical properties of the stratospheric aerosols (SSA). The studied cases presented here are from the PNE and ANYSO events, as they are two of the most documented cases of PyroCb stratospheric injections of aerosols.

The Pacific Northwest Event occured during the 2017 summer fire season, during which several PyroCbs injected smoke into the stratosphere, for a total aerosol particle mass of 0.2 Tg (0.1 - 0.3 Tg according to Peterson et al. (2018) and 0.18 - 0.35 Tg according to Torres et al. (2020). The aerosols were injected at 13 km (Khaykin et al. (2018); Christian et al. (2019); Yu et al. (2019)), travelled the Northern Hemisphere with parts of them self-lofting for several months, and high amounts of smoke were observed in the lower stratosphere for more than 4 months (Peterson et al. (2018)).

The Australian New Year Super Outbreak occured in December 2019 and January 2020, caused by record breaking wildfire and pyroCb activity. Two distinct outbreaks happened on December 31 (phase 1) and January 5 (phase 2), with phase 1 injecting 0.2 - 0.8 Tg (Khaykin et al. (2020); Peterson et al. (2021)) which is 2 to 3 times higher than the PNE injection, and phase 2 injecting 0.1 - 0.3 Tg. In phase 1, aerosols were injected at 15 - 16 km (Kablick III et al. (2020); Khaykin et al. (2020)), part of which were observed to rise for 3 months up to 35 km.

From these two wildfire events, we focus on self-lofting SCVs in the stratosphere (in the following we will either call these SCVs or just plumes). We focus on the main self-lofting plume from PNE, and the main plume from ANYSO.

To track the two SCVs we use the method described in Khaykin et al. (2020), based on observations by CALIOP (Winker et al. (2010)) and OMPS-LP (Jaross et al. (2014)). The Ozone Mapping and Profiler Suite Limb Profiler (OMPS-LP) on the Suomi National Polar-orbiting Partnership (Suomi-NPP) satellite, measures limb-scattered sunlight, from which aerosol extinction profiles and ozone number density profiles are retrieved. The Cloud-Aerosol Lidar with Orthogonal Polarization (CALIOP) is a lidar on board the CALIPSO mission that provides high-resolution vertical profiles of aerosols and clouds in the troposphere and low stratosphere. In this study we use the aerosol profiles from both CALIOP/OMPS-LP to track the SCVs and compute their SAOD (Stratospheric Aerosol Optical Depth) and geometrical thickness, as well as position and potential temperature.

Fig. 1 top panel shows the trajectories of the two plumes. The PNE plume's tracked trajectory (blue circles) starts at 14 km above northern Canada on August 16^{th} 2017. The plume then travelled the Northern Hemisphere for 3 months, going to lower latitudes towards Europe and the Himalaya during the first month and then staying in the 20-30°N latitude band, travelling westward. It self-lofted up to 24 km in 3 months. The ANYSO plume's tracked trajectory (red squares) starts above New-Zeland on January 3^{rd} 2020. It then travelled the Southern Hemisphere for 3 months in the 25-60°S latitude band, self-lofting from 15km to almost 32 km, with its top going over 35 km.

Altitude, potential temperature and integrated SAOD of the SCVs are shown on the lower panel of Fig. 1. The optical thickness

https://doi.org/10.5194/egusphere-2026-2006
Preprint. Discussion started: 22 May 2026

of PNE's plume is initialy high at 0.6, but decreases steeply during the first month of ascension, resulting in a decreasing heating rate $\dot{\theta}$ over time. For the ANYSO plume, the initial SAOD is comparable at 0.4, but then decreases more slowly, with a constant heating rate (in terms of potential temperature), $d\theta/dt = \dot{\theta} \approx 5$ K.day^{-1}.

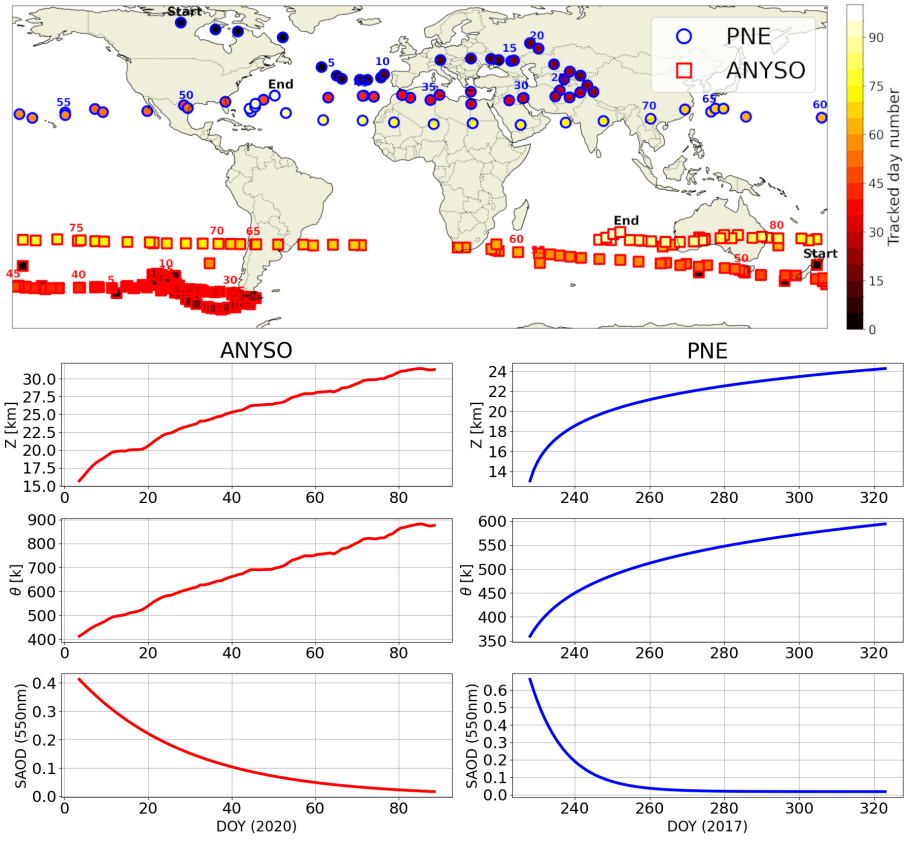

Figure 1. Trajectories (top panel) of the two main SCVs from ANYSO (red) and PNE (blue) events. The start/end of both trajectories are indicated, as well as the number of days of tracking. In the lower panel, altitude (top plot), potential temperature θ (middle plot) and in-plume optical thickness SAOD at 550nm (bottom) along the trajectories of the plume is also shown.

2.2 Optical properties of the aerosols

To be able to compute the heating rates of each case we need to know the optical and microphysical properties of the aerosols : in our case the refractive index as well as the size distribution. The parameters we use were measured by Ohneiser et al. (2020a) and Ansmann et al. (2021) for ANYSO, when it passed over Chile in 2020, and by Hu et al. (2019) for PNE, as it went over France in 2017. In both cases, these properties were obtained by ground-based, multi-wavelengths Raman lidars. The properties we use are shown in Table. 1, and as can be seen the uncertainties on the imaginary part of the refractive index are quite high, and lead to relatively large intervals of SSA values. In the rest of this study and to allow for better comparisons,

https://doi.org/10.5194/egusphere-2026-2006
Preprint. Discussion started: 22 May 2026

we will use the range [0.01,0.04] for the imaginary part of the refractive index in both cases. In sections 2.3 and 2.4 we show how heating rates vary for this range, as well as study their sensitivity to the mean radius of the size distribution.

For these computations, we suppose the refractive indexes of the aerosols to be spectrally constant, and we use them prior to the radiative computations to determine the SSA and asymmetry parameter of the aerosols, using a Mie routine. The SSA and asymmetry parameter used in the heating rates computations are spectrally dependant (shown at 550nm in Table 1). These properties are assumed to be constant over time, as we assume the plumes' chemical composition to remain stable after a couple days after the injection (Ansmann et al. (2021)).

Case	ANYSO	PNE
Size distribution (log normal parameters)	mean = 0.3 µm std = 1.26	mean = 0.24 µm std = 1.36
Re(refractive index)	1.48	1.55
Im(refractive index)	0.01 - 0.03	0.01 - 0.04
Single Scattering Albedo SSA_{550} range	0.95 - 0.86	0.95 - 0.83
Assymetry parameter g_{550} range	0.74 - 0.78	0.70 - 0.74
Reference	Ansmann et al. (2021)	Hu et al. (2019)

Table 1. Aerosol optical and microphysical properties used in this study. SSA and assymetry parameters were computed with a Mie routine using the size distribution and refractive indices.

2.3 Radiative modeling

To constrain the SSA values of the aerosols for each studied case, we model the plumes' heating rates $\dot{\theta}$ with the radiative modeling tool ARTDECO (Atmospheric Radiative Transfer Database for Earth Climate Observation model developed and maintained at the Laboratoire d'Optique Atmosphérique (LOA), distributed by the data center AERIS/ICARE (http://www.icare.univ-lille1.fr/projects/artdeco) which uses the one-dimensional discrete model DISORT (Stamnes et al. (2000)) as a radiative solver, as presented in Fig. 2. For each plume, we use the tracked trajectory obtained from observations, aerosol optical parameters shown previously, as well as various datasets to take into account the environment of the plume : collocated ERA5 atmospheric profiles (Hersbach et al. (2020)), extended up to 120km by the AFGL standard profiles (Anderson et al. (1986)), and MODIS datasets for the underyling cloud cover (product MCD06COSP, Team et al. (2022)) and surface albedo (product MCD43C3, Schaaf et al. (2002)). For each computation, the radiative model is used twice, in the longwave ([4, 500µm]) and shortwave

https://doi.org/10.5194/egusphere-2026-2006
Preprint. Discussion started: 22 May 2026

([0.2, 4µm]). Five atmospheric gases are taken into account , H_2O, O_3, O_2, CO_2 and CH_4, with k-distributions for their optical properties. The radiative computations are made hourly, with the corresponding local zenithal angle. A similar method was used by Ohneiser et al. (2020b) and Sellitto et al. (2022). The daily heating rate $\dot{T}$ (in terms of temperature) is computed as $\dot{T} = dT/dt = dF/dz \times D_{day}/(\rho_{air} \times c_{p,air})$, where dT/dz is the net radiative heating rate in the plume layer, D_{day} is the duration of a day in seconds, ρ_{air} is the air density and $c_{p,air}$ is the air heat capacity. The heating rate in terms of potential temperature is then $\dot{\theta} = \dot{T} \times (P_0/P)^{R/c_{p,air}} = \dot{T} \times (P_0/P)^{0.286}$, where R is the specific gas constant of the air. In the following, heating rate will refer to $\dot{\theta}$.

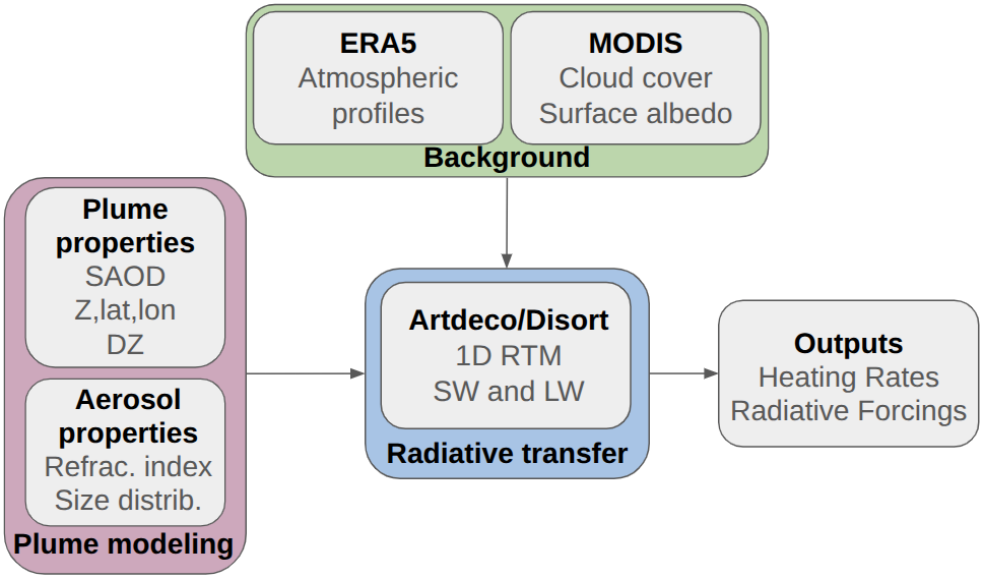

Figure 2. Methodology used to compute the plumes heating rates with the radiative model ARTDECO using the DISORT scheme. DZ is the geometrical thickness of the plume. See text for more details.

https://doi.org/10.5194/egusphere-2026-2006
Preprint. Discussion started: 22 May 2026

3 Results

In this section we present the results obtained with the radiative model presented above. We first show how different parameters can influence the self-lofting process, then discuss how different values of the SSA of the aerosols impact their heating rates. We then compute the global radiative forcings of the ANYSO stratospheric injection of 2020.

3.1 Parametric sensitivities

Several parameters have a significant impact on heating rates computations (Ohneiser et al. (2020a)). Fig. 3 shows the parametric sensitivity corresponding to some of them in the case of the ANYSO plume. Heating rates were computed for a base case (same orange line in all panels) with SSA = 0.9 (Im(refind)=0.02), all-sky conditions, geometrical thickness DZ = 10 km, and mean radius of the size distribution $r_g = 0.3$ µm. For each panel a different parameter was changed to show the sensitivity of the heating rates. Top left panel shows the impact of all-sky conditions on the heating rates compared to clear-sky (blue line) : an underlying bright surface such as clouds reflects part of the incoming solar radiation back to the plume, increasing the heating rate compared to a darker surface. In our case this corresponds to an increase of 2 K.day^{-1}. The geometrical thickness DZ of the plume is also a crucial parameter to compute the heating rates : for a given SAOD, changing DZ has a direct linear impact on the heating rates, as the shortwave flux absorbed by the plume will heat an atmospheric layer of height DZ. Top right panel of the figure shows that going from a constant DZ = 10 km to 5 km (blue line) almost multiplies by 2 the computed heating rates. In this study we find that this parameter has the largest impact on the heating rates. We also study the water vapor anomaly inside the plume compared to the stratospheric background (bottom left panel). It was measured 3 times higher in the ANYSO plume (Khaykin et al. (2020), written as H2Omulti = 3 in the figure bottom left panel, with H2Omulti = 1(blue line) corresponding to no water vapor anomaly (for the PNE plume it was measured at H2Omulti=2). This parameter can also impact the computed values of the heating rate, as the anomaly in water vapor inside the plume increases its longwave outgoing radiation, cooling it and reducing the heating rate, which corresponds to a difference of 1 K.day^{-1} in this case. The impact of the mean radius r_g of the size distribution of the aerosols is shown in the bottom right panel. For a given refractive index, reducing the mean radius from 0.4 µm to 0.2 µm increases the SSA from 0.87 to 0.91, hence reducing the heating rates.

https://doi.org/10.5194/egusphere-2026-2006
Preprint. Discussion started: 22 May 2026

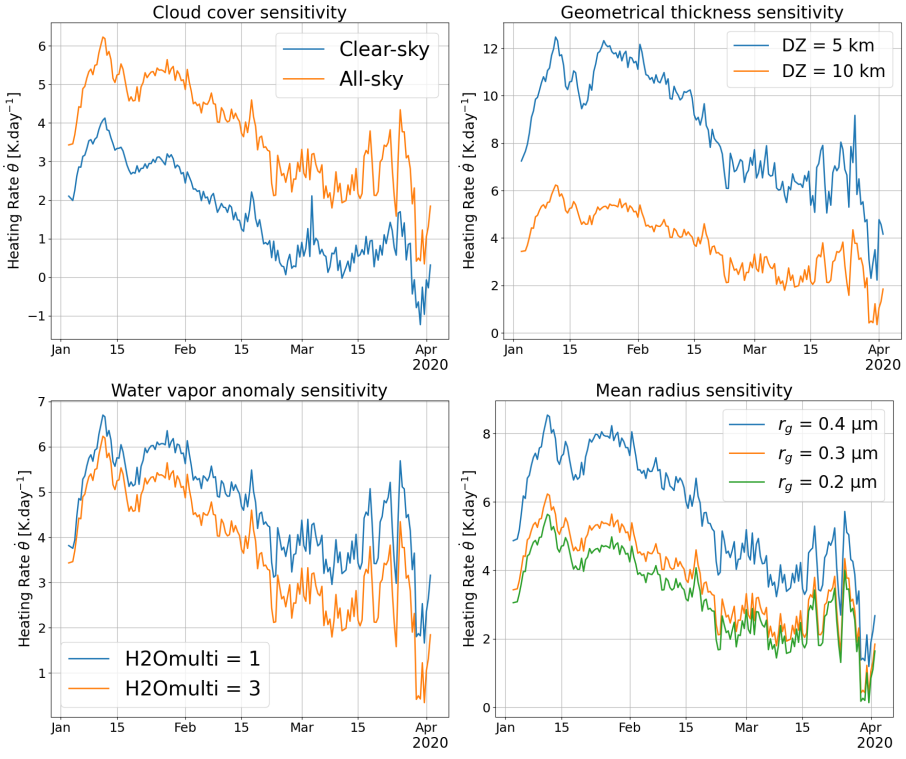

Figure 3. Parametric sensitivities of the heating rate $\dot{\theta}$ for the ANYSO plume. Studied parameters are clouds (top left), geometrical thickness DZ of the plume (top right), water vapor anomaly inside the plume (bottom left) and mean radius of the aerosols' size distribution (bottom right). The base case (in orange) is the same in each panel.

3.2 Heating rates and discussion

In this section, the cloud cover is taken into account, as well as water vapor anomaly and surface albedo. The size distributions used for each case are shown in Table. 1. The heating rates are then computed for different values of the imaginary part of the refractive index, corresponding to different values of the SSA. Computed heating rates are shown on Fig. 4 for the ANYSO plume (left) and the PNE plume (right). For each case, a dotted line shows the observed heating rates $\dot{\theta}$, derived from the potential temperature profiles of Fig. 1.

For both cases, the expected SSA range allows us to compute heating rates close to the observations. For the ANYSO plume the computed heating rates are similar to the observed ones but with a slightly different trend : observed heating rates are constant, when heating rates computed with a constant SSA decrease with time, as the optical depth of the plume also decreases. Overall, an SSA of 0.90 to 0.95 allows for the best reproduction of the observed heating rates. An SSA varying with time could be considered to tackle the trend discrepancy, from an initial SSA of 0.95, decreasing to about 0.90 over time. This would mean relaxing the hypothesis of constant optical properties, with aerosols getting darker over time during this 3 months period. Given a constant refractive index, such a change of SSA could also be caused by an evolution in the size

https://doi.org/10.5194/egusphere-2026-2006
Preprint. Discussion started: 22 May 2026

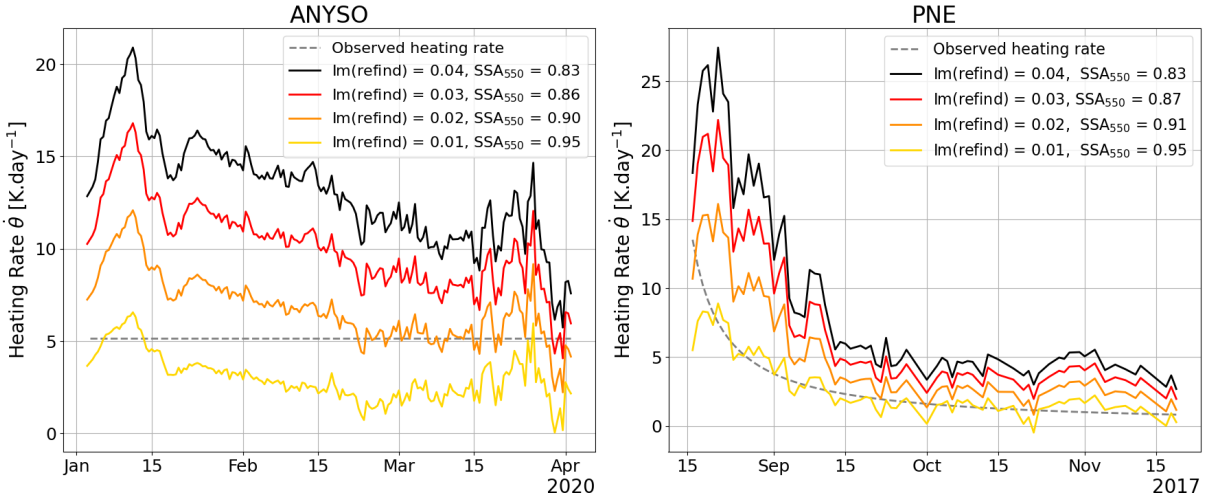

Figure 4. All-sky heating rates computed for different values of SSA for the ANYSO plume (left) and the PNE plume (right).

distribution of the aerosols, and we suggest there could be a growth of the aerosols' mean radius. Indeed, as shown previously in Fig. 3, aerosols' growth causes a decrease of their scattering efficiency at considered wavelengths, and thus leads to lower SSA, which could help stabilizing the heating rates over time. More work would be required to study this aspect which goes beyond the scope of this paper. For the PNE plume the most accurate SSA we found with this method is 0.95. The steep decrease of the SAOD during the first month after the injection is causing a similar trend for the observed heating rate, well reproduced in the computations. To conclude, we found our method is able to broadly reproduce the observed heating rates for the two studied plumes within the range of expected optical parameters, but observational uncertainties on key parameters (the geometrical thickness of the plumes and the evolution of the aerosols' SSA and size distribution) prevent us for now to reach higher precision. Our best estimates for the SSA of the SCVs' aerosols based on these results is 0.95 for PNE and 0.90 - 0.95 for ANYSO.

3.3 Global radiative forcings of stratospheric aerosols from ANYSO

In this section we compute the global radiative forcings of stratospheric aerosols for the year 2020. The ANYSO event from the Australian wildfires of late December 2019 and early January 2020 was the only major stratospheric injection in the Southern Hemisphere (SH), and we present here our estimates for its global radiative impact over 2020.

The dataset used here is stratospheric aerosol extinction vertical profiles for 2020, at a monthly resolution and zonally averaged with a 1 degree resolution in latitude. It was obtained from OMPS-LP (Jaross et al. (2014)). Fig. 5 top-left panel shows the monthly-zonal mean integrated SAOD (at 550nm) over the Southern Hemisphere for 2019-2020. The annual mean SAOD for 2020 is 0.02 and is mostly due to ANYSO's injections in late December 2019 - early January 2020, with a continuous decrease during the following year. The radiative model used in this section is the same as previously. Like before, underlying

https://doi.org/10.5194/egusphere-2026-2006
Preprint. Discussion started: 22 May 2026

clouds are taken into account. On average over 2020 and for SH, the total cloud fraction is higher than 50% at all latitudes, especially at latitudes higher than 40°S where most of the SAOD from ANYSO was injected. For the Southern Hemisphere the annual average of the cloud cover is 63%.

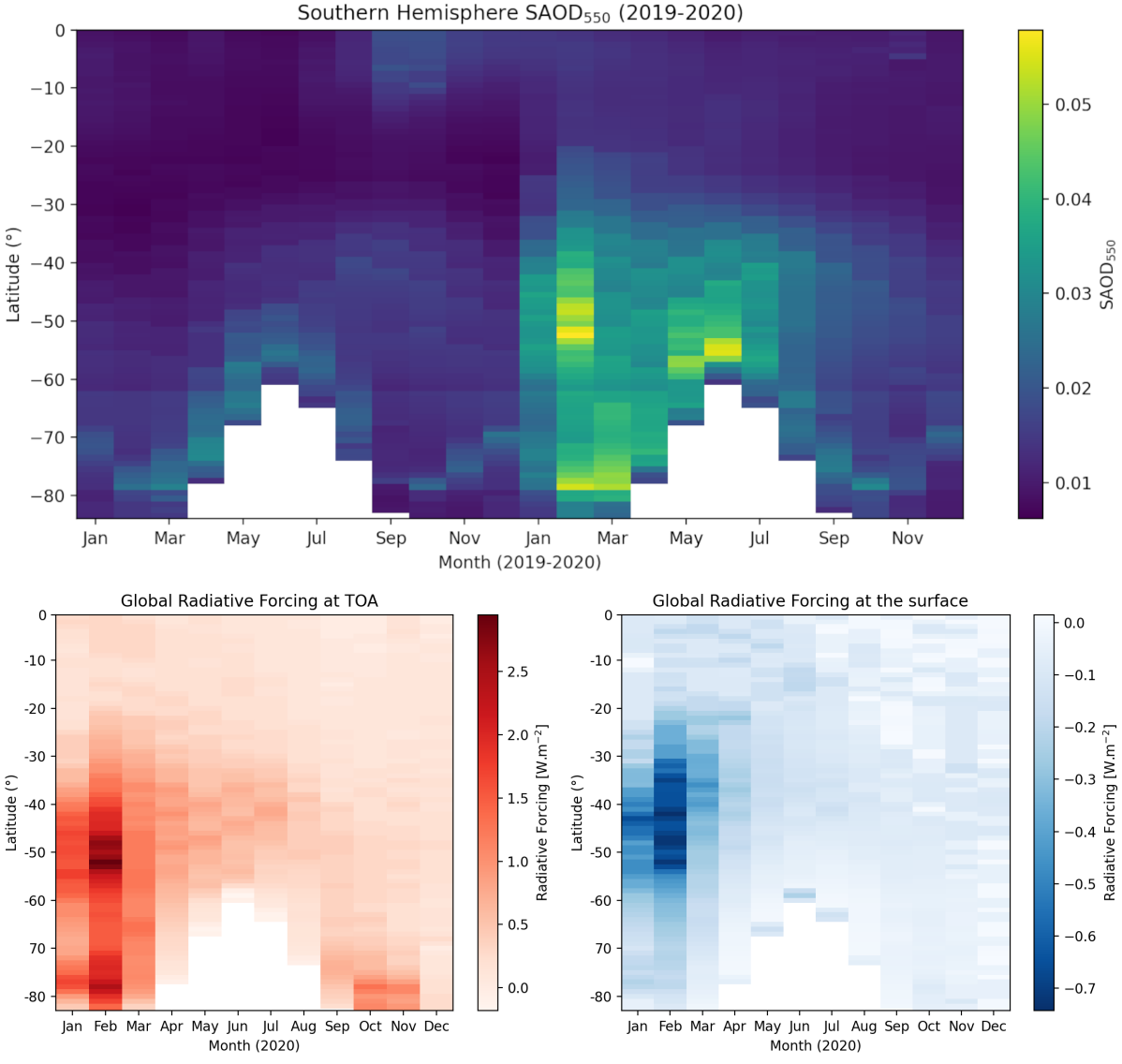

Figure 5. Top panel shows the global SAOD at 550 nm computed from OMPS-LP extinction profiles, for 2019 and 2020 in the Southern Hemisphere. Bottom panels show computed radiative forcings : at TOA (left) and at the surface (right). Radiative forcings were computed in all-sky conditions with SSA = 0.90 for the aerosols (Im(refind)=0.02).

https://doi.org/10.5194/egusphere-2026-2006
Preprint. Discussion started: 22 May 2026

We compute the radiative forcings at the surface and at TOA, for ANYSO aerosols in the Southern Hemisphere as :

$$RF_{surf} = (F_{surf}^{ANYSO,\downarrow} - F_{surf}^{ANYSO,\uparrow}) - (F_{surf}^{bkg,\downarrow} - F_{surf}^{bkg,\uparrow})$$

$$RF_{TOA} = F_{TOA}^{bkg,\uparrow} - F_{TOA}^{ANYSO,\uparrow}$$

with F being the radiative flux. F^{bkg} indicates the computation was made only with the background aerosols, that are assumed to have the same extinction coefficient profiles as in 2019 : $k_{bkg} = k_{ext}(2019, t, z)$. On the other hand F^{ANYSO} indicates that the computations were made with the same background aerosols, as well as the aerosols injected by ANYSO, with their extinction profile $k_{ANYSO} = k_{ext}(2020, t, z) - k_{ext}(2019, t, z)$. For the ANYSO aerosols the radiative properties used are the same as in the previous section. For the background aerosols and similarly as done by Duchamp et al. (2023) and Sellitto et al. (2025), we consider background aerosols to be droplets of a H2SO4/H2O mixture at a weight proportion of 70%, which corresponds at 213K to a refractive index of 1.44 + $i10^{-6}$ (Biermann et al. (2000)). The size distribution of the background aerosols is taken as a log-normal distribution with mean radius $r_g = 0.07$ µm and a standard deviation of $\sigma_g = 1.86$ (Sellitto and Legras (2016)).

Fig. 5 bottom panels show the SH all-sky TOA (left) and surface (right) radiative forcings computed for SSA = 0.90 (Im(refind)=0.02). For the RF at TOA we find positive values, with a local SH annual mean of 0.38 W.m^{-2}, as the aerosols' absorption reduces the cloud albedo effect, hence warming the atmosphere. For the surface RF we find negative values, with a local SH annual mean of -0.12 W.m^{-2}, which is due to the SW albedo effect of the aerosols, a lesser radiative flux reaching the surface in their presence. On a global scale (both hemispheres) this results in a RF at TOA of 0.19 W.m^{-2}, and at the surface of -0.06 W.m^{-2} from the stratospheric aerosols injected by ANYSO in the SH. For both radiative forcings, the effect of the aerosols is larger in February when the optical extinction is at its peak.

Since the computations shown here are made offline (not a part of a GCM), the quick adjustment of the stratospheric temperatures triggered by the shortwave heating of the aerosols is not taken into account, which makes the radiative forcings shown here direct (or instantaneous). The effective radiative forcing (ERF) at TOA is expected to be lower due to the stratospheric temperature adjustment causing LW cooling. According to Smith et al. (2018); Liu et al. (2022); Shine et al. (2022) this effect can be of the same order of magnitude than the SW RF at TOA itself. In the next sections, we discuss the impact of different SSA values on the radiative forcings, the effect of clouds, as well as comparisons with global values found in the literature.

3.3.1 Top Of the Atmosphere radiative forcing

Fig. 6 top left panel shows the global TOA RF of the aerosols injected by ANYSO in the stratosphere over 2020. Results are shown for different SSA values, in all-sky (solid lines) and clear-sky (dotted lines). The values are averaged globally, showing the effect of SH SAOD on the energy balance at the top of the atmosphere. In clear-sky conditions (dotted lines), all values are negative, due to the albedo effect of the aerosols : compared to the cloud-free surface, the presence of the aerosols is reflecting more solar radiation towards space. This effect is based on the scattering of light by the aerosols and is larger at higher SSA values (SSA = 0.90 in orange and SSA = 0.95 in yellow). In all-sky conditions (solild lines), the effect is positive, as the aerosols' absorption of solar radiation reduces the albedo effect of clouds. The effect is larger for more absorbing aerosols with

https://doi.org/10.5194/egusphere-2026-2006
Preprint. Discussion started: 22 May 2026

lower SSA values (SSA = 0.86 in red, and SSA = 0.83 in black). In the previous section, we found an SSA between 0.90 and 0.95 was best to model the heating rates of ANYSO's main SCV. For these SSA values of 0.90 and 0.95, the annual mean global RF at TOA is respectively 0.19 W.m^{-2} and 0.08 W.m^{-2} in all-sky, and -0.17 W.m^{-2} to -0.12 W.m^{-2} in clear-sky.

For instantaneous SW RF at TOA, Heinold et al. (2022) find, for the first 3 months after ANYSO, values of 0.37 to 0.5 W.m^{-2} in all-sky, when we find 0.8 to 0.61 W.m^{-2} (using SSA = 0.83 to 0.86 to best compare with their parameters). In clear-sky conditions, Khaykin et al. (2020) and Sellitto et al. (2022) respectively estimate it at -0.31$\pm$0.09 and -0.35$\pm$ 0.21 W.m^{-2}, when we estimate it from -0.20 to -0.29 W.m^{-2}. As mentioned above, the ERF tends to be lower than the instantaneous RF due to stratospheric temperature adjustment. As shown by Smith et al. (2018); Liu et al. (2022); Shine et al. (2022), the resulting longwave emission can significantly reduce the radiative forcing at TOA. For the ANYSO injections, Yu et al. (2021) estimate it at -0.03 W.m^{-2} and Liu et al. (2022) at -0.17$\pm$0.02 W.m^{-2} (both in clear-sky). References discussed here are summarized in Table. 2, which also includes values derived from the PNE case.

To compare with the global values, the bottom left panel of Fig. 6 shows the local RF at TOA for ANYSO's main SCV that was studied in the previous section. The radiative forcing is computed in the same way, but values are local at TOA of the self-lofting plume. In clear-sky conditions (dotted lines), all values are negative, like previously found in the global case. For a 3-month average, the radiative forcing due to the SCV is -3.8 to -5.3 W.m^{-2} (for SSA = 0.90 to 0.95), with initial values peaking at -12 to -18 W.m^{-2} just after the injection, when the SAOD is the largest. In all-sky conditions, the RF at TOA is positive, with a 3-month average of 7.9 to 3.7 W.m^{-2} (for SSA = 0.90 to 0.95). The effect of clouds is once more crucial, both to the sign and amplitude of the TOA RF. It can be noted here that absolute values are meaningfully larger than in the global case, as local SAOD is much larger in the case of the individual SCV plume, where aerosol concentration is locally higher.

https://doi.org/10.5194/egusphere-2026-2006
Preprint. Discussion started: 22 May 2026

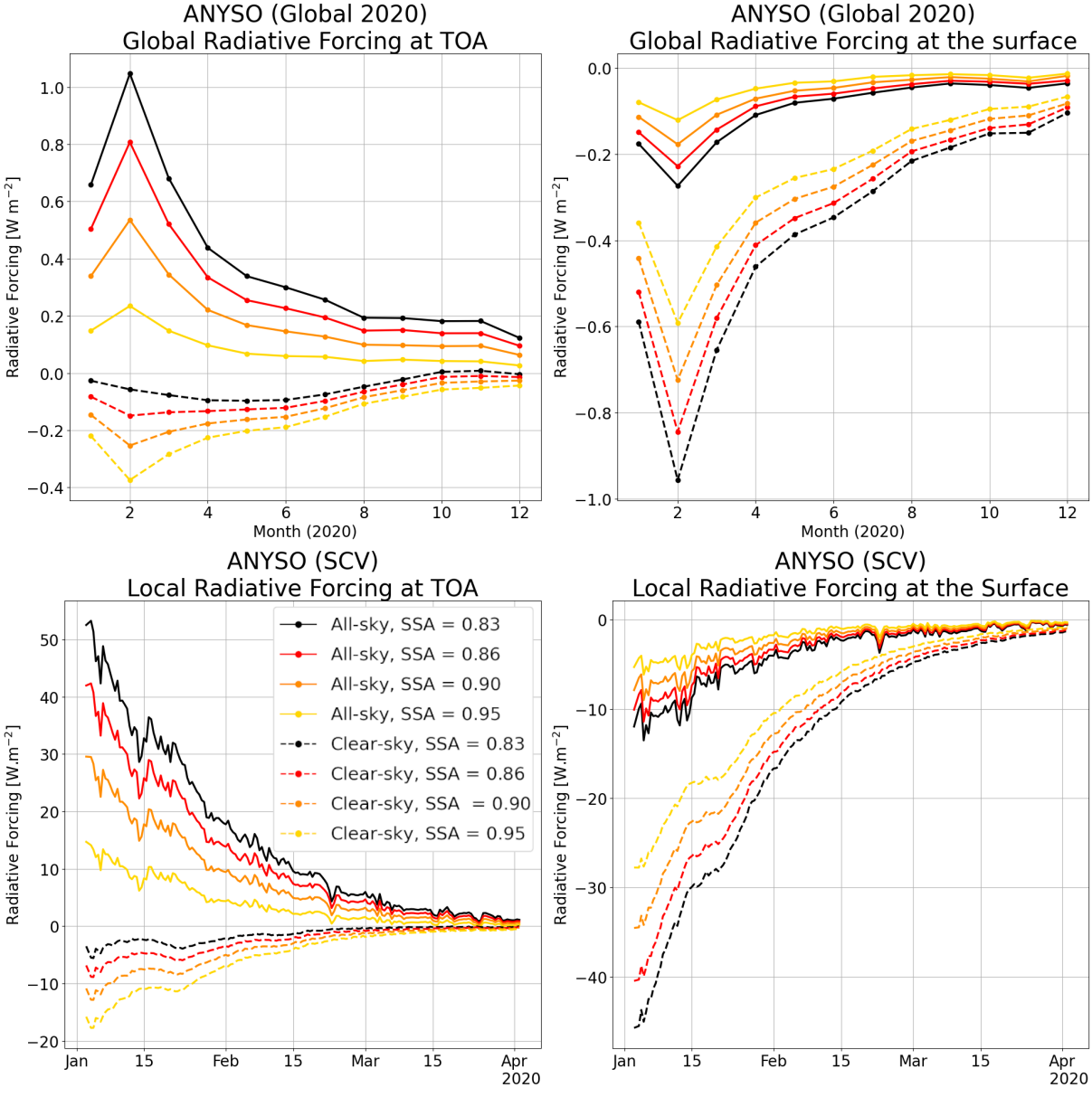

Figure 6. Global TOA radiative forcing caused by stratospheric aerosols in the Southern Hemisphere for 2020 (top panels). Bottom panels show local RF caused by ANYSO's main SCV. Solid lines represent all-sky conditions and dashed lines clear-sky conditions.

https://doi.org/10.5194/egusphere-2026-2006
Preprint. Discussion started: 22 May 2026

3.3.2 Surface radiative forcing

Fig. 6 top right panel shows the computed RF at the surface from the SH ANYSO aerosols. We find negative radiative forcings both in all-sky and clear-sky conditions. This is expected in both cases as the aerosols reflect and absorb part of the incoming shortwave radiation, reducing the incoming flux reaching the surface in both cases. In clear-sky conditions this effect is strong, but it is reduced in the presence of underlying clouds, by a factor of 4 to 6 in our case. For SSA values of 0.90 and 0.95, the mean global RF at the surface is respectively -0.06 W.m^{-2} and -0.04 W.m^{-2} in all-sky, and -0.29 W.m^{-2} and -0.24 W.m^{-2} in clear-sky.

For instant SW RF at the surface, Heinold et al. (2022) find, for the first 3 months after ANYSO, values of -0.42 to -0.5 W.m^{-2} in all-sky, when we find -0.21 to -0.17 W.m^{-2} (for SSA = 0.83 to 0.86). In clear-sky conditions, Khaykin et al. (2020); Sellitto et al. (2022) respectively estimate it at -0.98$\pm$0.17 and -0.94$\pm$0.26 W.m^{-2}, when we find -0.56 to -0.46 W.m^{-2}. Finally, the surface effective radiative forcing is also expected to be smaller due to stratospheric adjustment, e.g. Yu et al. (2021) estimate is -0.32 W.m^{-2} in clear-sky. References are summarized in Table. 2.

To compare with the global values, the bottom right panel of Fig. 6 shows the local RF at the surface for ANYSO's main SCV that was studied in the previous section. In clear-sky conditions (dotted lines), all values are negative, like previously found in the global case. For a three-month average, the local radiative forcing at the surface in all-sky conditions is positive with a values of -2.4 to -1.6 W.m^{-2} (for SSA = 0.90 to 0.95). In clear-sky conditions those values are -10.4 to -8.5 W.m^{-2}. Once again, the high optical thickness of the SCV compared to the global stratospheric injection by ANYSO causes much larger forcings locally.

Table 2. State of the art of the literature on PNE and ANYSO radiative forcings.

The Optical Properties column is not exhaustive as some of the models use their own parameterization for aerosols.

Publication	Case (clear-sky/all-sky)	Optical Properties	Radiative Model	Radiative Forcings [W.m^{-2}]
Christian et al. (2019)	PNE (all-sky)	BC/OC = 6%	CTM GEOS-CHEM + 4-stream RTM	SW TOA RF = 0.02 (global, instant)
Hu et al. (2019)	PNE (clear-sky)	refind = [1.5;1.6] + i [0.01;0.04] radius = 0.33µm	RTM GARLIC/GRASP	TOA RF ∈ {-3.5,-1.2} Surf RF ∈ {-14.5,-12.3}
Das et al. (2021)	PNE (all-sky)	BC/OC = 2.5% SSA(355nm)=0.75 SSA(532nm)=0.9	GEOS-AGCM	TOA RF = -0.03±0.01 Surf RF = -0.12±0.03
Liu et al. (2022)	PNE (clear-sky)	OM : refind =1.53+i0.0057 Sulfate : refind =1.43+i1e-8	GCM CESM1 + RRTMG	TOA RF = -0.04±0.02 (global annual mean)
Lee et al. (2023)	PNE (all-sky)	SSA~0.9	GCM E3SM	RF TOA 0.196 surf -0.295
Khaykin et al. (2020)	ANYSO (clear-sky)	SSA = 0.85 to 0.95 g=0.7	RTM SDisort	SW TOA RF -0.31±0.09 SW Surf RF -0.98±0.17
Yu et al. (2021)	ANYSO (clear-sky)	BC/OC=2%	GCM CESM + RTM CARMA	TOA RF -0.03 Surf RF -0.32
D'Angelo et al. (2022)	ANYSO (all-sky)	r=0.3µm	GCM CESM1/GEOS5	SW Surf RF = -3
Heinold et al. (2022)	ANYSO (all-sky)	OC/(OC+BC) = 5 to 8% SSA(550nm) = 0.82 to 0.85	GCM ECHAM6 + RRTMG	SW Surf RF ∈ [-0.5,-0.42] SW TOA RF ∈ [0.37,0.5]
Liu et al. (2022)	ANYSO (clear-sky)	OM : refind =1.53+i0.0057 sulfate : refind =1.43+i1e-8	CESM1 + RRTMG	TOA RF = -0.17±0.02 (global annual mean)
Sellitto et al. (2022)	ANYSO (clear-sky)	SSA = 0.85-0.95 g=0.5-0.7	RTM SDisort	TOA RF = -0.35±0.21 Surf RF = -0.94±0.26
Yu et al. (2023)	2014-2022 SAOD (clear-sky)	Yu et al. (2015)	GCM CESM + RTM CARMA	TOA RF = -0.18 TOA ERF = -37

https://doi.org/10.5194/egusphere-2026-2006
Preprint. Discussion started: 22 May 2026

4 Conclusion

We presented a study to evaluate the global radiative forcings of the stratospheric injections of aerosols by the ANYSO event over 2020. To do so, we first studied two cases of self-lofting Smoke-Charged Vortices from the 2017 PNE event and 2020 ANYSO event, in order to constrain the SSA of aerosols as well as identify key environment parameters impacting the heating rates of the plumes. We then applied our method to compute the global surface and TOA radiative forcing of stratospheric aerosols injected by ANYSO in 2020.

We used the ARTDECO radiative computations tool with the Disort radiative transfer scheme to compute heating rates of the self-lofting plumes and compared them to observations. We concluded that several factors have a strong impact on the heating rates : the SSA, which can vary with the imaginary part of the refractive index or with the size distributions of the aerosols; the geometrical depth of the plumes, which impacts linearly the heating rates, given the optical depth is known; and accounted for the cloud cover, which added 2 $K.day^{-1}$ to the heating rates for the ANYSO plume. To a lesser extent, in-plume water vapor anomaly also impacts the heating rates of the SCVs. Using this method, our best estimates for the SSA were 0.95 for the PNE plume and 0.90 - 0.95 for the ANYSO plume.

Using the same method we computed the total surface and TOA radiative forcings of stratospheric aerosols in the Southern Hemisphere in 2020 injected by the ANYSO event, compared to background stratospheric aerosols from 2019. Our computations were based on OMPS-LP extinction profiles. We found that taking into account the cloud cover for the surface radiative forcing can reduce its values by a factor of 5, and that it is even more essential for the TOA radiative forcing, where it changes its sign, going from negative in clear-sky to positive in all-sky conditions, while also changing its amplitude by a factor of 2 for the ANYSO case. Although the effect is qualitatively well known, many studies present only clear-sky radiative forcings for the ANYSO event, even though the average SH cloud cover is higher than 60%. Our estimate for the the global TOA radiative forcing of ANYSO over 2020 is 0.08 to 0.19 $W.m^{-2}$ in all-sky, and -0.17 to -0.12 $W.m^{-2}$ in clear-sky. For the surface radiative forcing our estimate is -0.04 to -0.06 $W.m^{-2}$ in all-sky and -0.29 to -0.24 $W.m^{-2}$ in clear-sky. With our method we were able to compute direct (instantaneous) radiative forcings, without taking into account the LW adjustment of the stratosphere. This effect could be added in a further study by involving GCMs to obtain definitive effective radiative forcing of the ANYSO event. Finally we showed that local RF for the individual main SCV plume injected by ANYSO is one order of magnitude larger, as the plume has higher optical thickness, due to its high aerosol concentration. Further work is needed to reconcile the global estimates of the radiative forcings to values local to individual plumes, where several plumes could be tracked during the same event using chemistry-transport models to account for the plumes dynamics, evolution of their composition as well as their radiative impacts.

Fueled by global warming, stratospheric injections of aerosols by extreme wildfires will likely become more frequent, with an increased impact on the atmosphere's radiative balance, and further work is needed to reduce uncertainties regarding the

https://doi.org/10.5194/egusphere-2026-2006
Preprint. Discussion started: 22 May 2026

composition of these aerosols (especially the evolution of their SSA) as well as their total radiative forcing, while taking into account key parameters such as cloud cover.

Code and data availability. The radiative modeling tool ARTDECO (Atmospheric Radiative Transfer Database for Earth Climate Observation) is distributed by the data center AERIS/ICARE (http://www.icare.univ-lille1.fr/projects/artdeco).

Author contributions. The study was performed by RL and was designed by RL, YD, FR, SK. The SCVs data was provided by SK. The radiative simulations were performed by RL and JB. All co-authors participated in the discussion of the results. RL wrote the manuscript and all co-authors contributed to its revision and editing.

Competing interests. The authors declare no competing interests.

Financial support. This research has been supported by the Agence National de la Recherche (grant 21-CE01-0028, PYROSTRAT) and the CDP-AREA Project from Université de Lille.

https://doi.org/10.5194/egusphere-2026-2006
Preprint. Discussion started: 22 May 2026

References

Allen, D. R., Fromm, M. D., III, G. P. K., and Nedoluha, G. E.: Smoke with Induced Rotation and Lofting (SWIRL) in the Stratosphere, Journal of the Atmospheric Sciences, 77, 4297 – 4316, https://doi.org/10.1175/JAS-D-20-0131.1, 2020.

Anderson, G. P., Clough, S. A., Kneizys, F., Chetwynd, J. H., and Shettle, E. P.: AFGL Atmospheric Constituent Profiles (0.120 km), Tech. Rep. AFGL-TR-86-0110, Air Force Geophysics Laboratory, 1986.

Ansmann, A., Ohneiser, K., Mamouri, R.-E., Knopf, D. A., Veselovskii, I., Baars, H., Engelmann, R., Foth, A., Jimenez, C., Seifert, P., and Barja, B.: Tropospheric and stratospheric wildfire smoke profiling with lidar: mass, surface area, CCN, and INP retrieval, Atmospheric Chemistry and Physics, 21, 9779–9807, https://doi.org/10.5194/acp-21-9779-2021, 2021.

Biermann, U., Luo, B., and Peter, T.: Absorption spectra and optical constants of binary and ternary solutions of H2SO4, HNO3, and H2O in the mid infrared at atmospheric temperatures, The Journal of Physical Chemistry A, 104, 783–793, 2000.

Boers, R., de Laat, A. T., Stein Zweers, D. C., and Dirksen, R. J.: Lifting potential of solar-heated aerosol layers, Geophysical Research Letters, 37, https://doi.org/https://doi.org/10.1029/2010GL045171, 2010.

Christian, K., Wang, J., Ge, C., Peterson, D., Hyer, E., Yorks, J., and McGill, M.: Radiative Forcing and Stratospheric Warming of Pyrocumulonimbus Smoke Aerosols: First Modeling Results With Multisensor (EPIC, CALIPSO, and CATS) Views from Space, Geophysical Research Letters, 46, 10 061–10 071, https://doi.org/https://doi.org/10.1029/2019GL082360, 2019.

Das, S., Colarco, P. R., Oman, L. D., Taha, G., and Torres, O.: The long-term transport and radiative impacts of the 2017 British Columbia pyrocumulonimbus smoke aerosols in the stratosphere, Atmospheric Chemistry and Physics, 21, 12 069–12 090, https://doi.org/10.5194/acp-21-12069-2021, 2021.

de Laat, A. T. J., Stein Zweers, D. C., Boers, R., and Tuinder, O. N. E.: A solar escalator: Observational evidence of the self-lifting of smoke and aerosols by absorption of solar radiation in the February 2009 Australian Black Saturday plume, Journal of Geophysical Research: Atmospheres, 117, https://doi.org/https://doi.org/10.1029/2011JD017016, 2012.

Duchamp, C., Wrana, F., Legras, B., Sellitto, P., Belhadji, R., and von Savigny, C.: Observation of the aerosol plume from the 2022 Hunga Tonga—Hunga Ha'apai eruption with SAGE III/ISS, Geophysical Research Letters, 50, e2023GL105 076, 2023.

D'Angelo, G., Guimond, S., Reisner, J., Peterson, D. A., and Dubey, M.: Contrasting Stratospheric Smoke Mass and Lifetime From 2017 Canadian and 2019/2020 Australian Megafires: Global Simulations and Satellite Observations, Journal of Geophysical Research: Atmospheres, 127, e2021JD036 249, https://doi.org/https://doi.org/10.1029/2021JD036249, 2022.

Fromm, M., Lindsey, D. T., Servranckx, R., Yue, G., Trickl, T., Sica, R., Doucet, P., and Godin-Beekmann, S.: The Untold Story of Pyrocumulonimbus, Bulletin of the American Meteorological Society, 91, 1193 – 1210, https://doi.org/10.1175/2010BAMS3004.1, 2010.

Guimond, S. R., Reisner, J., and Dubey, M.: The Dynamics of Megafire Smoke Plumes in Climate Models: Why a Converged Solution Matters for Physical Interpretations, Journal of Advances in Modeling Earth Systems, 15, e2022MS003 432, https://doi.org/10.1029/2022MS003432, _eprint: https://onlinelibrary.wiley.com/doi/pdf/10.1029/2022MS003432, 2023.

Heinold, B., Baars, H., Barja, B., Christensen, M., Kubin, A., Ohneiser, K., Schepanski, K., Schutgens, N., Senf, F., Schrödner, R., Villanueva, D., and Tegen, I.: Important role of stratospheric injection height for the distribution and radiative forcing of smoke aerosol from the 2019–2020 Australian wildfires, Atmospheric Chemistry and Physics, 22, 9969–9985, https://doi.org/10.5194/acp-22-9969-2022, 2022.

Hersbach, H., Bell, B., Berrisford, P., Hirahara, S., Horányi, A., Muñoz-Sabater, J., Nicolas, J., Peubey, C., Radu, R., Schepers, D., et al.: The ERA5 global reanalysis, Quarterly journal of the royal meteorological society, 146, 1999–2049, 2020.

https://doi.org/10.5194/egusphere-2026-2006
Preprint. Discussion started: 22 May 2026

Hu, Q., Goloub, P., Veselovskii, I., Bravo-Aranda, J.-A., Popovici, I. E., Podvin, T., Haeffelin, M., Lopatin, A., Dubovik, O., Pietras, C., et al.: Long-range-transported Canadian smoke plumes in the lower stratosphere over northern France, Atmospheric Chemistry and Physics, 19, 1173–1193, 2019.

Jaross, G., Bhartia, P. K., Chen, G., Kowitt, M., Haken, M., Chen, Z., Xu, P., Warner, J., and Kelly, T.: OMPS Limb Profiler instrument performance assessment, Journal of Geophysical Research: Atmospheres, 119, 4399–4412, https://doi.org/https://doi.org/10.1002/2013JD020482, 2014.

Kablick III, G. P., Allen, D. R., Fromm, M. D., and Nedoluha, G. E.: Australian PyroCb Smoke Generates Synoptic-Scale Stratospheric Anticyclones, Geophysical Research Letters, 47, e2020GL088 101, https://doi.org/https://doi.org/10.1029/2020GL088101, e2020GL088101 10.1029/2020GL088101, 2020.

Khaykin, S., Legras, B., Bucci, S., Sellitto, P., Isaksen, L., Tencé, F., Bekki, S., Bourassa, A., Rieger, L., Zawada, D., Jumelet, J., and Godin-Beekmann, S.: The 2019/20 Australian wildfires generated a persistent smoke-charged vortex rising up to 35 km altitude, Communications Earth & Environment, 1, 1–12, https://doi.org/10.1038/s43247-020-00022-5, number: 1 Publisher: Nature Publishing Group, 2020.

Khaykin, S., Bekki, S., Godin-Beekmann, S., Fromm, M. D., Goloub, P., Hu, Q., Josse, B., Laeng, A., Meziane, M., Peterson, D. A., Pelletier, S., and Thouret, V.: Stratospheric impact of the anomalous 2023 Canadian wildfires: the two vertical pathways of smoke, Atmospheric Chemistry and Physics, 25, 14 551–14 571, https://doi.org/10.5194/acp-25-14551-2025, 2025.

Khaykin, S. M., Godin-Beekmann, S., Hauchecorne, A., Pelon, J., Ravetta, F., and Keckhut, P.: Stratospheric Smoke With Unprecedentedly High Backscatter Observed by Lidars Above Southern France, Geophysical Research Letters, 45, 1639–1646, https://doi.org/https://doi.org/10.1002/2017GL076763, 2018.

Lee, H.-H., Lundquist, K. A., and Tang, Q.: Pyrocumulonimbus Events Over British Columbia in 2017: An Ensemble Model Study of Parameter Sensitivities and Climate Impacts of Wildfire Smoke in the Stratosphere, Journal of Geophysical Research: Atmospheres, 128, e2022JD037 648, https://doi.org/https://doi.org/10.1029/2022JD037648, e2022JD037648 2022JD037648, 2023.

Lestrelin, H., Legras, B., Podglajen, A., and Salihoglu, M.: Smoke-charged vortices in the stratosphere generated by wildfires and their behaviour in both hemispheres: comparing Australia 2020 to Canada 2017, Atmospheric Chemistry and Physics, 21, 7113–7134, https://doi.org/10.5194/acp-21-7113-2021, 2021.

Liu, C.-C., Portmann, R. W., Liu, S., Rosenlof, K. H., Peng, Y., and Yu, P.: Significant Effective Radiative Forcing of Stratospheric Wildfire Smoke, Geophysical Research Letters, 49, e2022GL100 175, https://doi.org/10.1029/2022GL100175, _eprint: https://onlinelibrary.wiley.com/doi/pdf/10.1029/2022GL100175, 2022.

Ohneiser, K., Ansmann, A., Baars, H., Seifert, P., Barja, B., Jimenez, C., Radenz, M., Teisseire, A., Floutsi, A., Haarig, M., Foth, A., Chudnovsky, A., Engelmann, R., Zamorano, F., Bühl, J., and Wandinger, U.: Smoke of extreme Australian bushfires observed in the stratosphere over Punta Arenas, Chile, in January 2020: optical thickness, lidar ratios, and depolarization ratios at 355 and 532 nm, Atmospheric Chemistry and Physics, 20, 8003–8015, https://doi.org/10.5194/acp-20-8003-2020, 2020a.

Ohneiser, K., Ansmann, A., Baars, H., Seifert, P., Barja, B., Jimenez, C., Radenz, M., Teisseire, A., Floutsi, A., Haarig, M., Foth, A., Chudnovsky, A., Engelmann, R., Zamorano, F., Bühl, J., and Wandinger, U.: Smoke of extreme Australian bushfires observed in the stratosphere over Punta Arenas, Chile, in January 2020: optical thickness, lidar ratios, and depolarization ratios at 355 and 532 nm, Atmospheric Chemistry and Physics, 20, 8003–8015, https://doi.org/10.5194/acp-20-8003-2020, publisher: Copernicus GmbH, 2020b.

Peterson, D. A., Campbell, J. R., Hyer, E. J., Fromm, M. D., Kablick III, G. P., Cossuth, J. H., and DeLand, M. T.: Wildfire-driven thunderstorms cause a volcano-like stratospheric injection of smoke, NPJ climate and atmospheric science, 1, 30, 2018.

https://doi.org/10.5194/egusphere-2026-2006
Preprint. Discussion started: 22 May 2026

Peterson, D. A., Fromm, M. D., McRae, R. H., Campbell, J. R., Hyer, E. J., Taha, G., Camacho, C. P., Kablick III, G. P., Schmidt, C. C., and DeLand, M. T.: Australia's Black Summer pyrocumulonimbus super outbreak reveals potential for increasingly extreme stratospheric smoke events, NPJ climate and atmospheric science, 4, 38, 2021.

Peterson, D. A., Berman, M. T., Fromm, M. D., Servranckx, R., Julstrom, W. J., Hyer, E. J., Campbell, J. R., McHardy, T. M., and Lambert, A.: Worldwide inventory reveals the frequency and variability of pyrocumulonimbus and stratospheric smoke plumes during 2013–2023, npj Climate and Atmospheric Science, 8, 325, 2025.

Schaaf, C. B., Gao, F., Strahler, A. H., Lucht, W., Li, X., Tsang, T., Strugnell, N. C., Zhang, X., Jin, Y., Muller, J.-P., Lewis, P., Barnsley, M., Hobson, P., Disney, M., Roberts, G., Dunderdale, M., Doll, C., d'Entremont, R. P., Hu, B., Liang, S., Privette, J. L., and Roy, D.: First operational BRDF, albedo nadir reflectance products from MODIS, Remote Sensing of Environment, 83, 135–148, https://doi.org/https://doi.org/10.1016/S0034-4257(02)00091-3, the Moderate Resolution Imaging Spectroradiometer (MODIS): a new generation of Land Surface Monitoring, 2002.

Sellitto, P. and Legras, B.: Sensitivity of thermal infrared nadir instruments to the chemical and microphysical properties of UTLS secondary sulfate aerosols, Atmospheric Measurement Techniques, 9, 115–132, 2016.

Sellitto, P., Belhadji, R., Kloss, C., and Legras, B.: Radiative impacts of the Australian bushfires 2019–2020 – Part 1: Large-scale radiative forcing, Atmospheric Chemistry and Physics, 22, 9299–9311, https://doi.org/10.5194/acp-22-9299-2022, 2022.

Sellitto, P., Belhadji, R., Legras, B., Podglajen, A., and Duchamp, C.: The optical properties of the stratospheric aerosol layer perturbation of the Hunga Tonga–Hunga Ha'apai volcano eruption of 15 January 2022, Atmospheric Chemistry and Physics, 25, 6353–6364, 2025.

Shine, K. P., Byrom, R. E., and Checa-Garcia, R.: Separating the shortwave and longwave components of greenhouse gas radiative forcing, Atmospheric Science Letters, 23, e1116, https://doi.org/https://doi.org/10.1002/asl.1116, 2022.

Smith, C. J., Kramer, R. J., Myhre, G., Forster, P. M., Soden, B. J., Andrews, T., Boucher, O., Faluvegi, G., Fläschner, D., Hodnebrog, , Kasoar, M., Kharin, V., Kirkevåg, A., Lamarque, J.-F., Mülmenstädt, J., Olivié, D., Richardson, T., Samset, B. H., Shindell, D., Stier, P., Takemura, T., Voulgarakis, A., and Watson-Parris, D.: Understanding Rapid Adjustments to Diverse Forcing Agents, Geophysical Research Letters, 45, 12,023–12,031, https://doi.org/https://doi.org/10.1029/2018GL079826, 2018.

Stamnes, K., Tsay, S.-C., Wiscombe, W., and Laszlo, I.: DISORT, a general-purpose Fortran program for discrete-ordinate-method radiative transfer in scattering and emitting layered media: documentation of methodology, 2000.

Team, M. A. S. et al.: MODIS (Aqua/Terra) Cloud Properties Level 3 monthly, 1x1 degree grid, NASA Level 1 and Atmosphere Archive and Distribution System Distributed Active Archive Center (DAAC) data set, pp. MCD06COSP_M3_MODIS–062, 2022.

Torres, O., Bhartia, P. K., Taha, G., Jethva, H., Das, S., Colarco, P., Krotkov, N., Omar, A., and Ahn, C.: Stratospheric Injection of Massive Smoke Plume From Canadian Boreal Fires in 2017 as Seen by DSCOVR-EPIC, CALIOP, and OMPS-LP Observations, Journal of Geophysical Research: Atmospheres, 125, e2020JD032 579, https://doi.org/10.1029/2020JD032579, _eprint: https://onlinelibrary.wiley.com/doi/pdf/10.1029/2020JD032579, 2020.

Winker, D., Pelon, J., Coakley Jr, J., Ackerman, S., Charlson, R., Colarco, P., Flamant, P., Fu, Q., Hoff, R., Kittaka, C., et al.: The CALIPSO mission: A global 3D view of aerosols and clouds, Bulletin of the American Meteorological Society, 91, 1211–1230, 2010.

Yu, P., Toon, O. B., Bardeen, C. G., Mills, M. J., Fan, T., English, J. M., and Neely, R. R.: Evaluations of tropospheric aerosol properties simulated by the community earth system model with a sectional aerosol microphysics scheme, Journal of Advances in Modeling Earth Systems, 7, 865–914, https://doi.org/https://doi.org/10.1002/2014MS000421, 2015.

Yu, P., Toon, O. B., Bardeen, C. G., Zhu, Y., Rosenlof, K. H., Portmann, R. W., Thornberry, T. D., Gao, R.-S., Davis, S. M., Wolf, E. T., de Gouw, J., Peterson, D. A., Fromm, M. D., and Robock, A.: Black carbon lofts wildfire smoke high into the stratosphere to form a

https://doi.org/10.5194/egusphere-2026-2006
Preprint. Discussion started: 22 May 2026

persistent plume, Science, 365, 587–590, https://doi.org/10.1126/science.aax1748, publisher: American Association for the Advancement of Science, 2019.

Yu, P., Davis, S. M., Toon, O. B., Portmann, R. W., Bardeen, C. G., Barnes, J. E., Telg, H., Maloney, C., and Rosenlof, K. H.: Persistent Stratospheric Warming Due to 2019–2020 Australian Wildfire Smoke, Geophysical Research Letters, 48, e2021GL092 609, https://doi.org/10.1029/2021GL092609, _eprint: https://onlinelibrary.wiley.com/doi/pdf/10.1029/2021GL092609, 2021.

Yu, P., Portmann, R. W., Peng, Y., Liu, C.-C., Zhu, Y., Asher, E., Bai, Z., Lu, Y., Bian, J., Mills, M., Schmidt, A., Rosenlof, K. H., and Toon, O. B.: Radiative Forcing From the 2014–2022 Volcanic and Wildfire Injections, Geophysical Research Letters, 50, e2023GL103 791, https://doi.org/https://doi.org/10.1029/2023GL103791, e2023GL103791 2023GL103791, 2023.